Liquid Crystals
Publication details, including instructions for authors and subscription information:
http://www.informaworld.com/smpp/title~content=t713926090

de Gennes' triclinic smectics - not so far-fetched after all

Nattaporn Chattham[a]; Eva Korblova[b]; Renfan Shao[a]; David M. Walba[b]; Joseph E. Maclennan[a]; Noel A. Clark[a]
[a] Liquid Crystal Materials Research Center and Department of Physics, University of Colorado, Boulder, Colorado, USA [b] Liquid Crystal Materials Research Center and Department of Chemistry and Biochemistry, University of Colorado, Boulder, Colorado, USA

Online publication date: 18 November 2009

To cite this Article Chattham, Nattaporn , Korblova, Eva , Shao, Renfan , Walba, David M. , Maclennan, Joseph E. and Clark, Noel A.(2009) 'de Gennes' triclinic smectics - not so far-fetched after all', Liquid Crystals, 36: 10, 1309 — 1317
To link to this Article: DOI: 10.1080/02678290903306458
URL: http://dx.doi.org/10.1080/02678290903306458

Liquid Crystals,
Vol. 36, Nos. 10–11, October–November 2009, 1309–1317

Taylor & Francis
Taylor & Francis Group

INVITED ARTICLE

de Gennes' triclinic smectics – not so far-fetched after all

Nattaporn Chattham[a]*, Eva Korblova[b], Renfan Shao[a], David M. Walba[b], Joseph E. Maclennan[a] and Noel A. Clark[a]*

[a]*Liquid Crystal Materials Research Center and Department of Physics, University of Colorado, Boulder, Colorado 80309, USA;* [b]*Liquid Crystal Materials Research Center and Department of Chemistry and Biochemistry, University of Colorado, Boulder, Colorado 80309, USA*

(Received 12 May 2009; final form 29 May 2009)

Study of the optical symmetry of the high-temperature liquid crystal phase of the bent core molecule **NORABOW** produces the first direct evidence for a material having fluid layers with internally stabilised triclinic symmetry, exhibiting the SmCPG structure: spontaneous in-plane polar ordering as well as substantial coherent molecular tilt in two Euler angles, giving an optical dielectric tensor with none of the principal axes oriented in or normal to the layer plane. The resulting C_1 symmetry makes **NORABOW** layers the least symmetric fluids. This triclinic layer structure is found to be robust, depending little on the relative state of neighbouring layers or position relative to the air interface.

Keywords: liquid crystal; bent-core; triclinic

1. Introduction

In the introductory remarks on smectic liquid crystals of the 1975 edition of his famous book (*1*), de Gennes proposed the triclinic smectic structure:

> In the third type of biaxial smectics the tensor $\boldsymbol{Q}_{\alpha\beta}$ may have all three axes tilted (none of them retaining a simple orientation with respect to the layers). We shall use the label C_G (where G stands for generalized) for this rather far-fetched possibility.

Thus, for example, a lath-shaped parallelepiped representing the principal axes of a biaxial optical dielectric tensor of a smectic layer can orient such that none of its faces lie either normal or parallel to the layer plane, a structure that could, in principle, be formed by lath-shaped molecules. In the absence of macroscopic polarisation, such a layer, which we term SmCG, would have only inversion symmetry and would therefore belong to the triclinic Schoenflies point symmetry class C_i (*2*). If in addition the molecules were to have spontaneous *polar* ordering (SmCGP) they would then also lack inversion symmetry, and thus be chiral, belonging to the class C_1, of the least-symmetric fluids. Currently, the only known phases of such low symmetry are the triclinic crystals, belonging to space groups #1 (P1, having only the identity element), and #2 (P-1, having inversion and identity point symmetry elements). Among the phases having fluid degrees of freedom in which the symmetry has been directly probed, the fluid layered smectic liquid crystals of chiral molecules, in which the mean long molecular axis, **n**, is tilted relative to the layer normal, **z**, are of lowest symmetry. Such layers are of the monoclinic class C_2, with only a two-fold rotation axis, normal to the **n–z** plane (*3*), as verified by detailed optical probes of structure (see, for example, (*4*)).

Here we present direct observations of the optical and polarisation symmetries of three to five layer-thick freely suspended smectic films (*5*), obtaining unambiguous evidence for ordering into C_1 layers in a smectic phase of the bent core molecular compound **NORABOW** (Figures 1, 2) (*6*). **NORABOW** was designed on the structural theme that is already known to produce fluid smectics with spontaneous polar molecular orientational ordering (*7*), and chiral tilt of the molecular plane in the B2 phase (*8*). These are anti- (A) or syn- (S) ordered in adjacent layers to give the four basic SmCP phases, the SmC_SP_S, C_AP_A, C_SP_A and C_AP_S (Figure 3a, green shading (*8*, *9*). These were originally identified (*8*) and confirmed by precision measurement (*10*) to have smectic layers of C_2 symmetry, i.e. polarisation *normal* to the optic axis tilt plane, the universal geometry of all heretofore identified fluid tilted chiral smectics. We show that **NORABOW** layers are 2D translationally invariant fluids exhibiting three instabilities: collective polar molecular orientational ordering, and coherent rotation of the molecular plane about two orthogonal (Euler) axes. These angles are measured and found to be only weakly dependent on the state of neighbouring layers, the resulting C_1 character of each layer only weakly dependent on the state of, or for that matter presence or absence of, neighbouring layers, a consistent C_1 layer structure existing in a variety of interfacial

*Corresponding authors. Email: nattaporn.c@ku.ac.th; noel.clark@colorado.edu

ISSN 0267-8292 print/ISSN 1366-5855 online

DOI: 10.1080/02678290903306458
http://www.informaworld.com

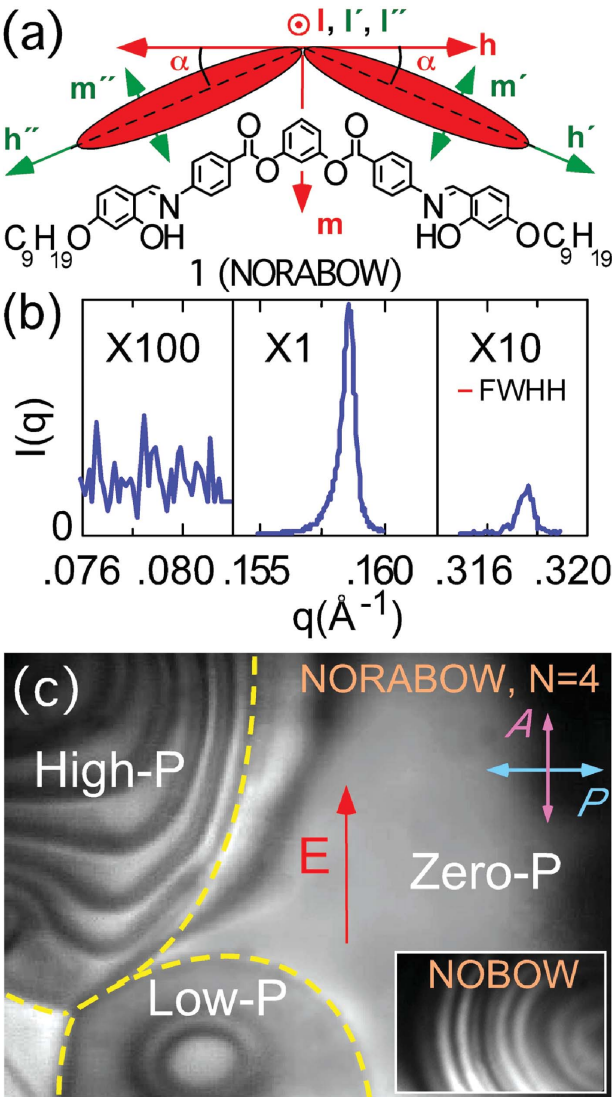

Figure 1. (a) The bent core molecule **NORABOW** sketched in the **h–m–l** molecular frame. The biaxial dielectric tensor is calculated by averaging two uniaxial sub-fragments diagonal respectively in the **h′–m′–l′** and **h″–m″–l″** frames (**h** – high, **m** – medium, **l** – low refractive index). (b) Powder X-ray diffraction at $T = 140°C$ in the fluid smectic phase of **NORABOW**, showing first- and second-order Bragg peaks, with no half-order reflection and the peaks resolution limited (red bars), indicative of monolayer ordering of planar (unmodulated) smectic layers. (c) Depolarised reflected light microscopy (DRLM) photomicrograph under crossed polarisers with obliquely incident illumination showing three areas with different states of **P** in a four-layer-thick film of **NORABOW**. The $P = 0$ area retains a smooth $\varphi(x,y)$ texture with a field applied, whereas field-stabilised 2π walls develop in the $P \neq 0$ areas. In a $P \neq 0$ B2 phase with **E** parallel to the polariser axis, the regions separating the 2π walls would be dark: so their bright appearance in **NORABOW** indicates a lower symmetry. (c, inset) DRLM photomicrograph under crossed polarisers with obliquely incident illumination of a **NOBOW** (*8*) winding pattern texture in the B2 SmC_SP_A phase showing the $C_{2\|}$ monoclinic symmetry pattern with two pairs of equal intensity peaks in each period of the ring pattern. Width of (c) = 400 μm. Width of inset = 400 μm.

environments. These results provide direct triclinic order parameter measurements to support claims of C_1 behaviour in bent core systems in which the layer structure and symmetry has not been established (*11–15*); in bent core phases in which sub-harmonic X-ray reflections indicate a bilayer unit cell and thus layers with alternating polarity along the layer normal (*16–18*); or in more complex, two dimensionally ordered phases (*19*).

2. Observations

X-ray diffraction (XRD) study of bulk powder samples and depolarised transmission light microscopy (DTLM) of freely suspended films were performed on the SmCPG phase of **NORABOW**, which has the bulk cooling phase sequence: isotropic (I) (177°C) SmCPG (99°C) SmX, and an I-SmCPG transition ~30°C higher in few layer thick films. XRD (Figure 1) shows that the SmCPG phase has a simple fluid lamellar structure with a layer spacing $d = 39.6$ Å, indicating that the molecules are tilted, since the extended molecular length is $L = 50$ Å. For a simple molecular rotation about **l** (Figure 1), the mean 'X-ray' tilt of the **h-m** molecular plane relative to layer normal **z** would be $\theta_{X\text{-ray}} = \cos^{-1}(d/L) = 38°$, a value which agrees with the results of bulk electro-optical measurements (*6*).

The response of four layer ($N = 4$) films to in-plane electric field, shown in Figure 1(c), revealed three distinct regions having different states of **P**, the in-plane polarisation: (i) $P = 0$; (ii) low-P ($P_L \sim 4$ nC/cm^2); and (iii) high-P ($P_H \sim 17$ nC/cm^2), as evidenced by the width $w = (K/PE)^{1/2}$ of the in-plane 2π walls of reorientation of φ stabilised by the field (*20*), where K is the Frank elastic constant in the one constant approximation. Of these three states, the $P = 0$ was most stable, tending to grow slowly in area at the expense of areas of non-zero P over periods of hours. By applying of a 20 Hz AC field it was possible to drive circular electrohyrodynamic flow of the films which wound up the orientation field $\varphi(x,y)$, generating areas in which the lines of constant $\varphi(x,y)$ were nested rings, with $\varphi(x,y)$ increasing approximately linearly with radius through many multiples of 2π after E was set to zero. Such ring structures, which could be formed in all three regions, as shown in Figure 2, along with field-induced textures such as in Figure 1(c), enabled the quantitative analysis of the dependence of the depolarised reflected light microscopy (DRLM) reflectivity $R(\beta,\varphi)$, the ratio of the depolarised to polarised reflected intensity, on φ and on β, the uncrossing angle of the analyser (Figure 3(c)). $R(\beta,\varphi)$ was measured vs. position through several rings of reorientation with $E = 0$. Typical ring pattern images are shown in Figure 2, along with corresponding plots of $R(\beta,\varphi)$ measured over 2π intervals in azimuthal orientation. Since $E = 0$ in these experiments, the origin in φ is not directly determined. However, an experimental φ

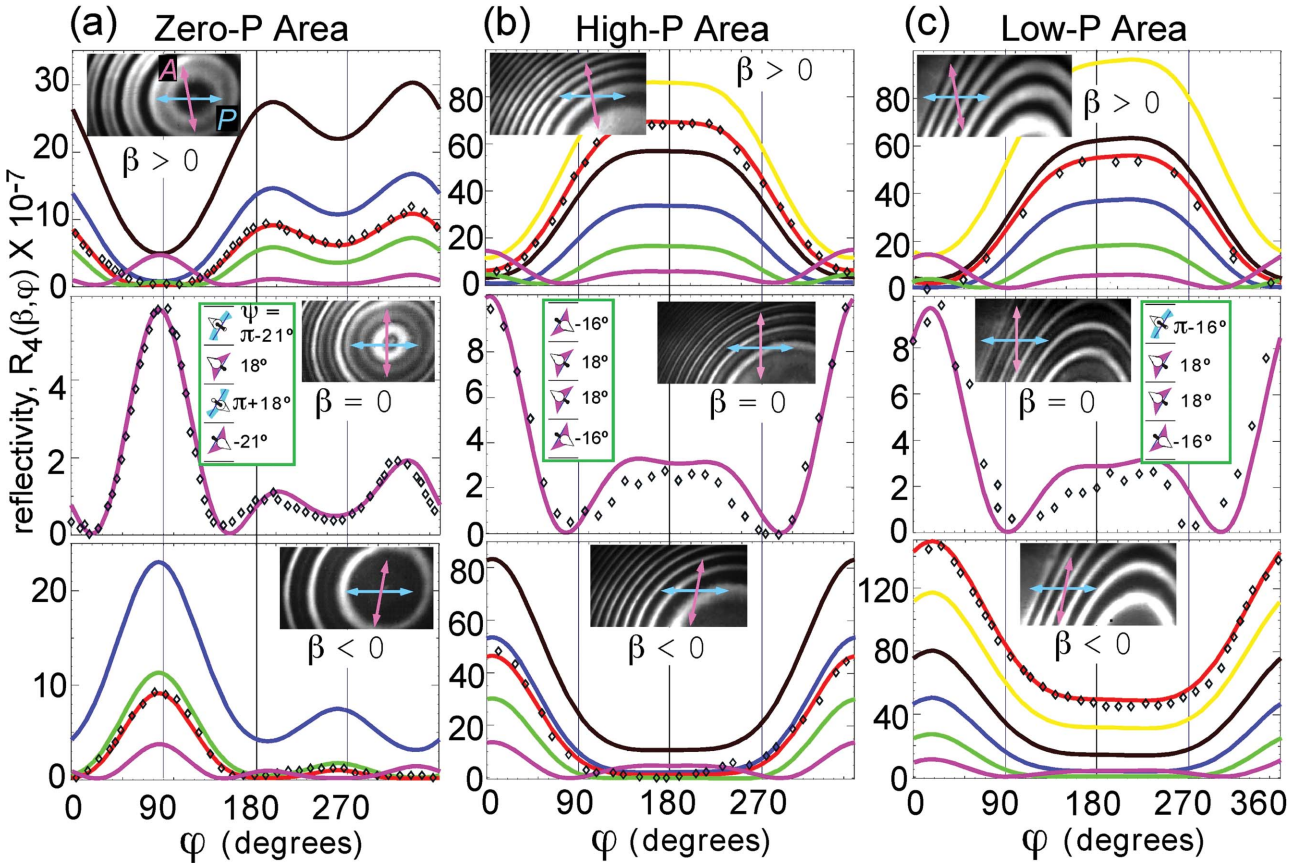

Figure 2. Model and experimental depolarised reflected light microscopy (DRLM) reflectivity, $R_4(\beta,\varphi)$, of a four-layer-thick **NORABOW** film at $T = 165°C$. Calculations are presented for analyser uncrossing angles $\beta = \pm 0.8°$(yellow), $\pm 0.6°$(black), $\pm 0.4°$(blue), $\pm 0.2°$(green), and 0°(pink). The experimental data are retrieved from winding pattern images such as those shown in the inset of each plot. Selected data (diamonds) and the fitted model (red) are presented for (a) $\beta = 0.29°$ and $\beta = -0.16°$, (b) $\beta = 0.33°$ and $\beta = -0.66°$, and (c) $\beta = 0.94°$ and $\beta = -0.50°$. The insets (green boxes) show schematic drawings of the structure of the best fit for each case. (a) An $N = 4$ film with $P = 0$ must consist of two (surface and interior) pairs of C_i symmetric layers and is thus achiral in DRLM (right-handed molecules are cyan, left-handed magenta). The surface and interior χ rotations, $|\chi_{surf}|$ and $|\chi_{in}|$, are nearly equal in magnitude but opposite in direction. *(**b**,**c**)* The high-*P* and low-*P* areas are obtained from the zero-*P* by flipping the handedness of one or two layers, respectively. In any of the above cases if $|\chi_{in}| = |\chi_{surf}|$ the average (DRLM-relevant) film structure becomes C_2 symmetric, making the fits quite sensitive to χ and, in particular, the difference $|\chi_{in}| - |\chi_{surf}|$ (see text). Width of photos = 400 μm.

can be obtained by field stabilisation of 2π walls as shown in Figure 1 by rotating the film such that **E** is in the plane of incidence. In this case the field-stabilised areas away from the 2π walls have **P** both parallel to **E** and in the plane of incidence, and thus have $\varphi = 0$, as defined in Methods. Comparison of the resulting intensity patterns through the 2π walls to those in Figure 2 (b) and (c) enables location of these field-stabilised areas in the $R_4(\beta,\varphi)$ patterns and thereby assignment of an experimental $\varphi = 0$ point on the measured $R_4(\beta,\varphi)$ that is used to plot the data in Figure 2 (b) and (c).

3. Analysis and discussion

Detailed comparison of the measured $R_N(\beta,\varphi)$ was made with the $R_N(\chi,\beta,\gamma)$ from the optical modelling. The insensitivity of $R_N(\chi,\beta,\gamma)$ to layer ordering (see Methods) enables a simple way of classifying film structures on the basis of the symmetry properties of DRLM $R_N(\beta = 0,\varphi)$ profiles, illustrated for all of the possible configurations of a film consisting of two SmCPG layers, (pink, blue shading in Figure 3(a)) (*21*). Here we start with the four distinct combinations of two SmCP layers (green shading in Figure 3(a), the SmC_SP_S, C_AP_A, C_SP_A, and C_AP_S (*8*, *22*, *23*), and perform the indicated SmCG rotations, i.e. rotations in χ (Figure 3(c)), to generate SmCG layers. The relative orientations about **z** will then relax according to Curie's principle, as indicated qualitatively in the view along **z** in Figure 3(a). The resulting average structures (gray shading, Figure 3(a)), characterised by their dielectric tensors (represented by red/orange/yellow orthorhombic parallelepipeds) and net polarisation vectors (black arrows), exhibit only six possibilities, as distinguished by symmetry (solid circles).

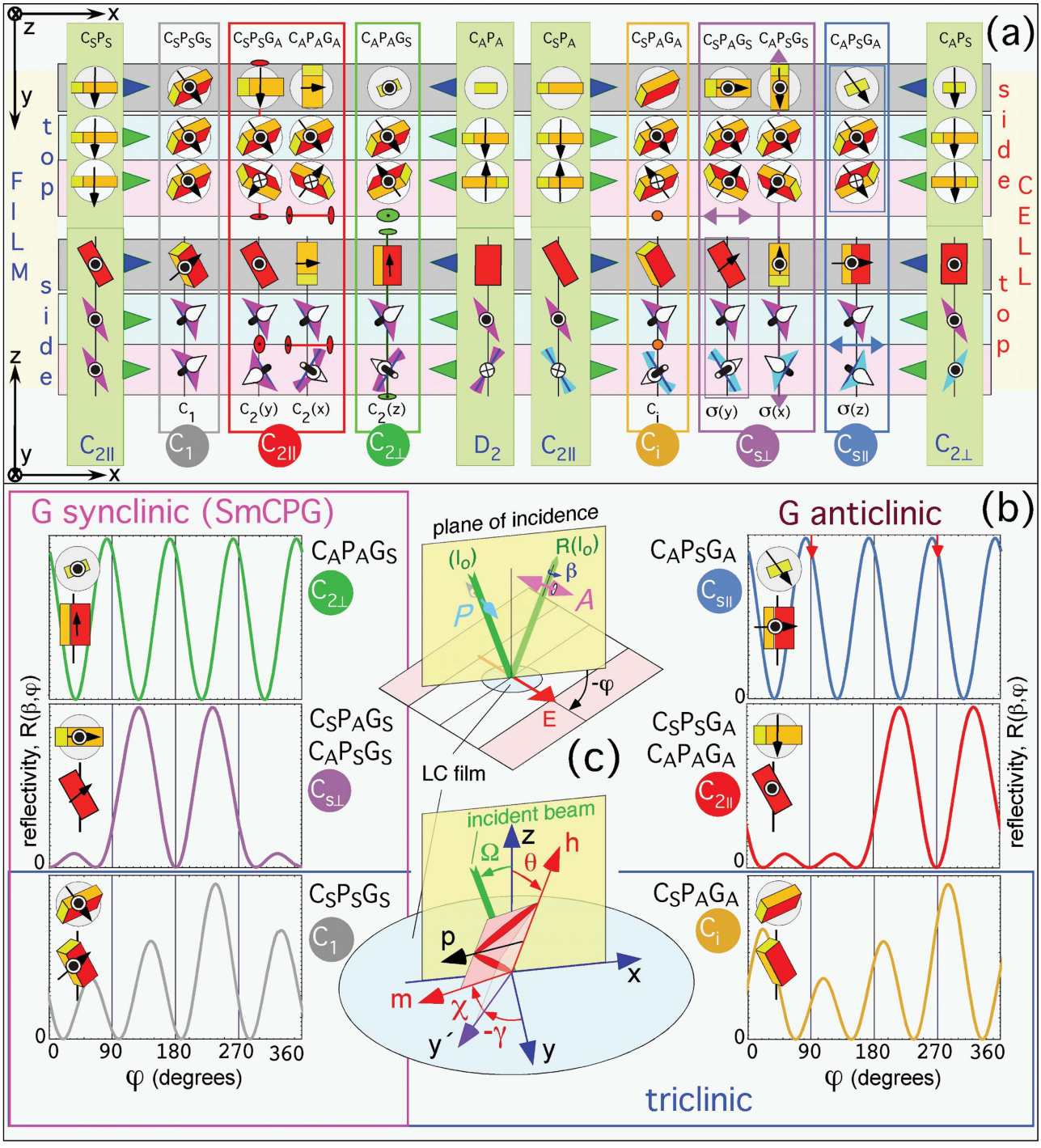

Figure 3. (a) Representations of the possible stable states of a pair of layers of bow-shaped molecules (pink and blue shading respectively). The top and side views are indicated for both the free FILM and electro-optical CELL geometries, the top view being that from the general direction of the incident light in each case. Here the optical dielectric tensors are represented as red/orange/yellow orthorhombic boxes, molecular dipole orientation is given by arrows, and molecular bow handedness by magenta or cyan colouring. Starting from the SmC_SP_S, C_AP_A, C_SP_A and C_AP_S structures of the B2 phase (green shading) (*8*), the SmCG rotation χ around the molecular long axis is performed (Figure 3(c)) in either a synclinic (G_S) or anticlinic (G_A) fashion, resulting in six possible bilayer structures (solid circles) distinguishable by the symmetry of their average dielectric tensor and net polarisation (gray shading). Also indicated are the symmetry operations taking one layer to the other, either twofold rotation (red/green), inversion (orange), or reflection (violet/blue). Once the χ rotations are made, relative azimuthal reorientation of the two layers reflecting this symmetry lowering will occur according to Curie's principle, indicated qualitatively in the view along **z**.

(Previous classifications (*7*, *8*, *23*) identified the CPG combinations in Figure 3(a) as eight possible SmCPG bilayer structures. However, among these there are only six distinct structures, as the $C_2(x)$, $C_2(y)$ and σ_x, σ_y pairs are of the same symmetry.)

These structures, and the plots of examples of the resulting calculated DRLM $R_2(\beta{=}0,\varphi)$ profiles in Figure 3(b), exhibiting their characteristic symmetries, show that oblique-incidence DRLM measurements in the presence of an in-plane field enable a direct probe of the point symmetry of the film and thereby an unambiguous classification of its structure if the layers are fluid. The two *triclinic* states, in which none of the principal axes lies in the film plane (C_i, C_1, Figure 3(b)), have $R_2(\beta, \varphi)$ profiles at $\beta = 0$ with four unequal peaks. Of these, the C_i ($P = 0$) state, with its opposing polarisations in the two layers, is an unavoidable consequence of the surface polarity along **z** of each layer due to having a smectic layer on one side and air on the other. This is to say that all two-layer SmC_SP_A films are by symmetry $SmC_SP_AG_A$, and thus are triclinic (C_i) rather than monoclinic (C_{2h}); and all two-layer SmC_AP_A films are by symmetry $SmC_AP_AG_A$, and thus monoclinic (C_2) rather than orthorhombic D_2, etc. However, in typical SmC_SP_A B2 materials, such as **NOBOW** (*8*), the rotation about χ is apparently so small that the deviation of $R(\beta = 0, \varphi)$ from the C_{2h} pattern (like the C_2 but with $P = 0$) has not been detectable (*8*, *10*). In contrast to the C_i, a two-layer film in the C_1 state ($P \neq 0$) requires a spontaneously broken symmetry to a net SmCPG structure. The two *monoclinic* states ($C_{2\|}$, $C_{s\perp}$, Figure 3(b), where the notations $\|$ and $\perp$ refer to the orientation of the symmetry operation relative to the film plane), in which one of the principal axes lie in the film plane, satisfy the reflection symmetry $R_2(\beta = 0,\varphi_o - \varphi) = R_2(\beta = 0,\varphi - \varphi_o)$, with $\varphi_o = \pi/2$ and 0 respectively, exhibiting one pair or two pairs (shown) of equal intensity $R_2(\beta = 0,\varphi)$ peaks, depending on the optical constants and angles. In analogy with the C_1 case, the $C_{2\|}$ state is also induced by surface polarity, whereas the $C_{s\perp}$ indicates a spontaneous net SmCPG ordering, the two cases being distinguished experimentally by whether the tilt plane aligns parallel or normal to the applied field. Analogous remarks apply to the structures with two principal axes in the film plane ($C_{2\perp}$, $C_{s\|}$) only one of which, the $C_{s\|}$, responds to in-plane field. Thus each of the six possibilities has a unique combination of optical symmetry and polarity. Finally, we note again that although the SmC_SP_S, C_AP_A, C_SP_A, and C_AP_S states can be found in bulk they are not expected in films, which must exhibit surface polarity-induced deformation toward the corresponding G_A states.

To the extent that layer order can be ignored, films with $N > 2$ can also be classified according to the six symmetries of Figure 3(b), which can be similarly distinguished by the study of $R_N(\beta = 0,\varphi)$, i.e. from the optical reflectivity and the response to field. This can be seen by considering the pink and blue shaded bands in Figure 3(a) to represent the net upper and lower half of a film with $N > 2$, rather than single layers. In order to obtain an overall structure more symmetric than a triclinic SmCPG, which occurs if the upper and lower half structures are unrelated by symmetry, one of the point operations indicated in *black* in Figure 3(a) ($C_2(x, y, \text{or } z)$, C_i, or C_s (x, y, or z)) must take the upper half of the film into the lower, a set which exhausts the possibilities and which yields just the six distinct DRLM signatures of Figure 3(b).

Application of these considerations to the **NORABOW** DRLM data of Figures 1 and 2 for $N = 4$ films shows immediately that the symmetry of the $P = 0$ state is C_i, and that the low-P and high-P areas are C_1. The $N = 4$ C_i symmetry state must be generated by pairs of inversion symmetric layers, which we have ordered with alternating handedness (magenta, cyan) in Figure 2(a). We note again, however, that the calculated $R_4(\beta,\varphi)$ are insensitive to the ordering of the layers, so that, for example, the outer layers could just as well be interchanged with the inner. As discussed above, for N even, the C_i symmetry is exactly that of a B2 SmC_SP_A film when the surface polarity along **z** is taken into account. However, comparison of $R_4(\beta = 0,\varphi)$ for the $P = 0$ C_i structure of $N = 4$ **NORABOW** films (Figure 2(a)), and that of the C_i

(b) The six possible local symmetries of a stack of SmCPG (C_1 symmetric) layers as distinguished by the principal axis orientations of their average dielectric tensor and by the orientation and magnitude of their net polarisation. Also presented is an example model depolarised reflected light microscopy (DRLM) reflectivity curve for each case, illustrating that the six states can be uniquely identified by the symmetries of their $R(\beta = 0,\varphi)$ curves and response to field, or lack thereof. Each case includes the top (gray circle) and side view average structure from (a). $R(\beta = 0,\varphi)$ has four equal intensity peaks if two principal axes are in the film plane (C_{2v}, C_{1h}), two pairs of equal intensity peaks if one principal axis is in the film plane (C_{1v}, C_2), and unequal intensity peaks if no principal axes are in the film plane (C_1, C_i). These symmetries and $R(\beta = 0,\varphi)$ characteristics cover all the possibilities for the average optical/polar properties of films of any number of SmCPG layers. (c) Geometry of the DRLM experiment (upper) showing incident light polarised perpendicular to plane of incidence, reflected light passed through an analyser uncrossed by an angle β, and the stage rotation φ of the plane of incidence from the electric field direction. The model calculation geometry (lower) illustrates the orientation of the molecular frame (**h**,**m**,**l**) relative to the lab frame (**x**,**y**,**z**), showing the SmC θ and SmCG χ rotations and the overall azimuthal orientation γ. In order to relate γ of the model calculation to φ in the experiment, the orientation of the in-plane component of the net model dipole moment must be calculated to determine azimuthal molecular orientation with an electric field applied.

SmC_SP_A structure of the B2 phase of **NOBOW** (*8*) in the inset of Figure 1(c), shows them to be quite different. The **NOBOW** C_i SmC_SP_A reflectivity exhibits no observable deviation from the pairs of large and small amplitude peaks expected for the SmC_SP_A in the absence of a SmCG χ rotation, i.e. for the simple $C_{2\|}$ SmC_SP_A (Figure 3(a)), which has the same optical signature as the $C_{2\|}$ or $C_{s\perp}$ (Figure 3(b)), but with $P = 0$. In addition, no such deviation is found in precision ellipsometric measurements (*10*). This implies that in **NOBOW** any χ rotation is quite small ($|\chi| < 2°$), whereas in **NORABOW** it is clearly much larger ($|\chi| \sim 20°$) in both the interior and outer layers. The inversion symmetry of the **NORABOW** C_i state ($P = 0$) makes it the simplest of the $N = 4$ structures to fit with a detailed optical model. We take θ to be the x-ray tilt $\theta = 38°$, then allow variation only of the χ rotation to SmCG for the inner (χ_{in}) and surface (χ_{surf}) layers in the structure sketched in Figure 2(a) (green box), where initially we make the azimuthal orientation γ (Figure 3(c)) of all of the layers the same, as it is in the SmC_SP_A (i.e. the molecular bowstrings are held in the same plane, although the surfaces would be expected in general to rotate in γ relative to the inner layers).

Effects of γ rotations of the layers away from the condition of having the bowstrings in a common plane have been explored to some extent, showing that small relative rotations $|\gamma| < 10°$ have little effect on $R(\beta,\varphi)$. Since $P = 0$, the field does not influence orientation and the calculated reflectivity $R_4(\chi,\beta,\gamma)$ can be freely shifted in γ while varying χ_{in} and χ_{surf} to obtain a best fit. The fits show that the SmCG rotations are of nearly equal magnitude in the inner and outer layers but in opposite directions [$|\chi_{in}| \sim |\chi_{surf}|$ (mod π)], with $|\chi_{in}| = 19°$ and $|\chi_{surf}| = 14°$ (mod π) rotations from the SmC_SP_A state, fitting the $R_4(\beta,\varphi)$ data well (Figure 2(a)). Note that in this C_i structure, if the SmCG rotations were of equal magnitude in the inner and outer layers [$|\chi_{in}| = |\chi_{surf}|$ (mod π)], then they would be equal and opposite within the pairs of layers of similar handedness (magenta or cyan). The symmetry of these pairs, and of the film overall, would then be C_2, and $R_4(\beta,\varphi)$ would be reflection symmetric about two φ values separated by 180° (as in Figure 3(b)). Thus the two smaller maxima in $R_4(\beta,\varphi)$ in Figure 2(a) merge and grow to equal the height of the large peak with a change of the interior layer χ_{surf} of only 5°, a change that gives $|\chi_{surf}| = |\chi_{in}| = 19°$ (mod π) and on-average (DRLM-relevant) C_2 symmetry. (If SmG tilts are tuned from $|\chi_{surf}| = |\chi_{in}| = 19°$ (mod π) to $|\chi_{surf}| = |\chi_{in}| = 0$ (mod π) then at some χ the two minima at $\varphi \neq 90°$, 270° in the C_2 pattern in Figure 3(b) will reappear to give the **NOBOW** ($|\chi_{surf}| = |\chi_{in}| \approx 0$) pattern of Figure 1(c) with four minima per ring. Thus the C_2 pattern, which is reflection symmetric about $\varphi = 90°$ and 270°, may have only the two symmetry-required minima at $\varphi = 90°$ and 270°.) Thus, the clearly non-C_2 nature of the $P = 0$ $R_4(\beta,\varphi)$ data of Figure 2(a) shows with high sensitivity that SmCG rotations must be different in the inner and outer layers and enables a precise measure of this difference.

The fact that the interior and surface layers have nearly the same χ rotation, differing by only ±2° from the average of $|\chi| \sim 16°$ (mod π) suggests that a large SmCG tilt in the range $14° < \chi < 19°$ is preferred internally by each layer, leading to the important conclusion that the preferred layer structure of **NORABOW** is SmCG, and suggesting that the choice of $|\chi| \sim 16°$ (mod π) is a good starting point for understanding the $N = 4$ states with $P \neq 0$. Recent experiments on single layer ($N = 1$) films yield $\theta \approx 40°$ and $\chi \approx 19°$ (*24*), essentially the same as the $N = 4$ film result, indicating that the NORABOW layers have an internally established triclinic structure. The simplest modification of the C_i structure we can make to attempt to match the $P \neq 0$ data is to flip the chirality of one of the layers (giving the low-P state), or two of the layers (giving the high-P state), a change that yields a polar C_1 symmetry with the same $R_4(\beta, \varphi)$ as the $P = 0$ state. Since the low-P and high-P reflectivities are quite similar, but somewhat different from the $P = 0$ state, additional variation of χ is then required to improve the fit. Specifically, increasing the average $|\chi_{surf}|$ to 16° (mod π) yields a good fit to $R_4(\beta,\varphi)$ (Figure 2 (b) and (c)). With the proposed chirality flips, the degeneracy of the environments of, for example, the two surface layers of the $P = 0$ state is lifted, so that, for example, in the homochiral high-P structure of Figure 2(b), there is no reason to expect that the χ of the two surface layers be the same, since one surface layer has its polarisation directed into the film and the other into the air. However, $R_4(\chi,\beta,\gamma)$ is not strongly sensitive to differences in $|\chi_{surf}|$ between the two surface layers, so they may actually have different χ tilts, as long as their average is $\langle|\chi_{surf}|\rangle \approx 16°$. Similar considerations apply to the interior layers, with $\langle|\chi_{in}|\rangle \approx 19°$. As for the zero-$P$ case, the fit is quite sensitive to the difference between χ_{surf} and χ_{in} since, if they are equal, the upper and lower pairs of layers would be $C_2(y)$, and the average film structure in Figure 2(b) would be $C_{2\|}$, in which case $R_4(\beta = 0,\varphi)$ would have minima at and be reflection symmetric about $\varphi = 90°$ and 270°.

For the $P \neq 0$ states, the direction and relative magnitude of the resulting polarisation can be obtained from the model by assigning each layer a unit vector polarisation **p** (Figure 3(c)) along the molecular 'arrows; in Figure 2. $\gamma(\varphi)$ is determined by assuming that $\mathbf{p}_{ave}$, the in-film plane component of

the average of **p** of the four layers, will then align along the applied field. This enables the calculated $R_4(\chi,\beta,\gamma)$ to be oriented in φ, with φ = 0 corresponding to the γ that puts $\mathbf{p}_{ave}$ in the plane of incidence (Figure 3(c)). The model $R_4(\chi,\beta,\gamma)$ curves in Figure 2 (b) and (c) are calculated on this basis. Accurate relative positioning in φ of the model and the experimental data is obtained in this way, indicating that simply averaging the unit molecular dipoles predicted by the model correctly yields the orientation of the net in-plane dipole density of a film.

As discussed above for several particular cases, the non-SmG ($\chi = 0$) bulk SmC_SP_S, C_AP_A, C_SP_A, and C_AP_S states cannot be present in films because they must be subject to deformation toward the corresponding $SmCPG_A$ states by surface polarity. However, both the data indicating that χ is small in **NOBOW** films (Figure 1(c) and (*10*)) and the relatively small differences between χ of interior and surface layers in **NORABOW** suggests that surface polarity effects, while favouring the G_A states, are too weak to change significantly the intrinsic structure of the layers. Thus, while **NOBOW** resists surface-induced change from its preferred monoclinic layer structure, **NORABOW** resists change from its preferred triclinic layer structure.

$N = 3$ and 5 films are multi-domain, and short-term observation shows that all domains respond to *E*-field and thus have net in-plane polarisation, as expected for an odd-*N* stacking of tilted chiral smectic layers (*25*). The $N = 3$ domains exhibit reflectivity patterns $R_3(\beta = 0,\varphi)$ similar in form to the those of the $N = 4$ films, suggestive of a three-layer stacking of layers with χ comparable to those found for $N = 4$.

4. Bulk structure and electro-optic behaviour

In order to investigate the structure of this smectic phase in bulk, **NORABOW** was filled into 4 μm-thick transparent capacitor electro-optic cells made from polyimide on indium-tin oxide coated glass plates, and observed via DTLM (these cells, which are commercially available from Displaytech (http://www.displaytech.com), have glass substrates with a 3.5- to 4.5-μm cell gap, coated with low-pretilt polyimide alignment layers). The rubbing directions on the two substrates are parallel. As reported previously (*6*) such cells give quasi-planar alignment into focal conics with extinction brushes along the polariser and analyser, indicative of an anticlinic ground state structure, similar to the C_AP_A state of **NOBOW** (Figure 3(a)), the prototypical B2 bent-core smectic. In **NOBOW** the ground state structures (C_AP_A and C_SP_A) grow in from the isotropic with two principal axes of **ε** parallel to the *x*–*z* plane of the plates, and thus the smectic layers, in the *x*–*y* plane, are normal to the plates, reflecting their respective $C_{2\|}$ (racemic) and D_2 (chiral) symmetries, both green-shaded in Figure 3(a). In contrast, DTLM experiments with tilted cells (Figure 4) show that **NORABOW** grows in with only *one* principal axis parallel to the plates, the one also lying parallel to the smectic layers, implying a ground state structure with tilt in the *y*–*z* plane (Figure 3(a)), either $C_{2\|}$ (chiral), $C_{s\perp}$ (racemic), or C_i (racemic) symmetries. Application of a sufficiently large electric field has two principal effects: (**i**) inducing a chiral ferroelectric response to a C_SP_S state, i.e. converting the racemic C_SP_A to C_SP_S as has been observed in **NOBOW** (*26*), and (**ii**) irreversibly standing the layers up to be parallel to the *x*–*y* plane, indicating that the

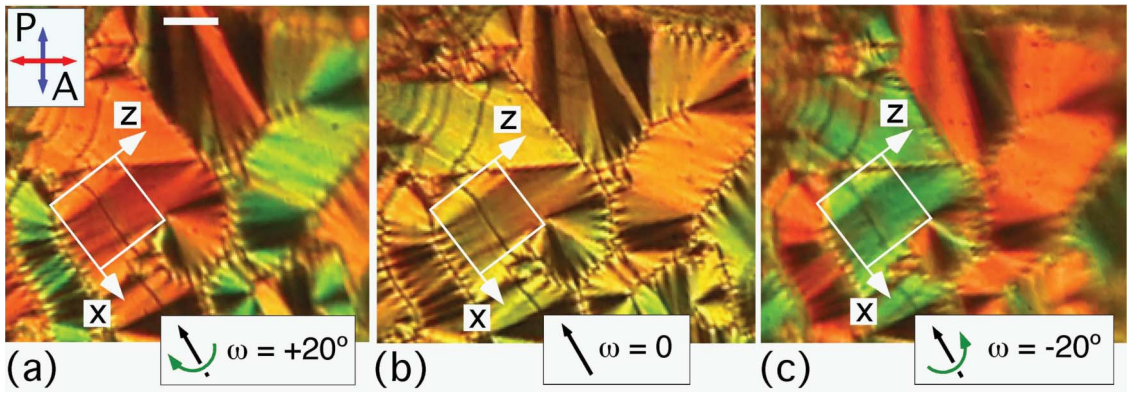

Figure 4. Depolarised transmission light microscopy images of an as-grown 4-μm thick **NORABOW** cell in white light for various orientations ω of the cell about the black arrow. The alternate yellow → green (yellow → orange) colour change of the domains indicates respectively a decrease (increase) in birefringence of $\Delta nd \approx 50$ nm from the second order yellow ($\Delta nd \approx 900$ nm) and thus opposite tilt of the domain's principal optic axes of magnitude $|\eta| \approx 21°$ about the local **x** direction (Figure 3(a)), indicated for the outlined domain. Scale bar = 50 μm.

SmCG χ tilt is anticlinic (G_A). This observation enables identification of the as-grown cell states as the $C_2(x)$ $SmC_AP_AG_A$ (chiral), obtained with field applied when cooling, the C_i $SmC_SP_AG_A$ (racemic), obtained in absence of field. The field-induced state is the $C_2(y)$ $SmC_SP_SG_A$ (chiral), obtained from the racemic above a threshold field $E_{th} \sim 14$ V/μm. This is another indication of the highly hysteretic nature of the overall organisation, also evident in the multistate nature of the films. Note that the $C_2(x)$ state has a polarisation $\mathbf{P}_x$ normal to the field $\mathbf{E}_y$ applied in the cell geometry, enabling a continuous field-induced transition to the $C_2(y)$ state and giving the previously reported analogue electro-optic behaviour (*6*). The tilt angle of the principal optical axis with respect to the x–z plane of the plates in the as-grown cells (η) can be determined from the birefringence change observed vs. cell rotation about **x**, with the result that $\eta \approx 21°$. Planned X-ray determination of the layer tilt in the as-grown cells will enable determination of the bulk χ.

5. Methods

5.1 X-ray diffraction

XRD experiments on powder samples were carried out on the Huber 4-circle goniometer on beamline X10A of NSLS at Brookhaven National Laboratory. This beamline employs a double-bounce Si monochromater and a Germanium 111 analyser to obtain wavevector resolution $\delta q \sim 0.0005$ Å^{-1} FWHH. Powder samples were contained in 1-mm diameter glass capillaries in a temperature-controlled chamber.

5.2 Freely suspended films

Freely suspended films, drawn in air with an integer number of smectic layers ($2 < N < 10$) and imaged with visible light DRLM (*20*), were employed as in (*8*) to probe the structure of the high-temperature (T) smectic phase of **NORABOW**. The I-SmCPG transition was ~10°C higher in few-layer-thick films. Films, with layer steps of uniform N, measured by laser reflectivity (*5*), were drawn in the high-temperature smectic phase over a 5-mm diameter hole in a glass cover slip coated with electrodes (pink areas, Figure 3(c)) for applying an in-plane electric field **E**, of magnitude 14.3 V/cm. DRLM observations with obliquely incident Ar+ laser light of wavelength $\lambda = 514$ nm (angle of incidence = 7°), illuminating a 300 μm diameter spot on the film and polarised normal to the plane of incidence. A crossed or slightly uncrossed analyser showed an optic axis tilted relative to the layer normal, and revealed the brush patterns characteristic of smooth optic axis reorientation $\varphi(x,y)$ about **z**, typical of films of fluid tilted smectics (*20*, *27*). For films with N in the range $2 < N < 10$, areas with even N were more easily generated. Of these the $N = 4$ areas were by far the most stable, expanding over periods of tens of minutes to cover the film and enabling observation over extended periods. Thus most of the data presented here are from $N = 4$ films, but with results from shorter-term observations of $N = 3$ and $N = 5$ films.

5.3 Modelling of the reflectivity

Theoretical reflectivities $R_N(\chi,\beta,\gamma)$, where N is the number of layers, were calculated using the Berreman 4 × 4 matrix method (*28*), assuming each layer of bent core molecules to consist of two halves about its midplane, each half a uniaxial slab of distinct optic axis direction (*29*).The uniaxial sublayers are given the dielectric constants of DOBAMBC ($\varepsilon'_l = 2.2$, $\varepsilon'_m = 2.2$, $\varepsilon'_h = 2.9$), as these, when used for **NOBOW**, give the correct indices of refraction for its B2 phase (*10*). The laboratory frame dielectric tensor of one bent core molecular layer is obtained by starting with the optical uniaxes of the two sublayers along the layer normal (**h**, **m**, and **l** respectively along **z**, **y**, and **x**, (Figure 3(c)) and rotating them about **l** by $\alpha = \pm 24°$ respectively (Figure 1), obtained from Gaussian calculations of the 3-ring core of **NORABOW** and **NOBOW** (*30*) and the extrapolated thickness of the core sub-layer in **NOBOW** (*30*). Then the rotation χ about **h** θ about **y**, and ultimately γ about **z** are performed to obtain $R(\theta\chi,\beta,\gamma)$ (Figure 3(c)). (Note that although three Euler angles specify molecular orientation (Figure 3(b)), the azimuth γ is irrelevant because we have no control over the γ to be adopted by a molecule – the packing takes care of this, so that orientations that superimpose by suitably changing γ are to be considered the same. This means that there are only two angles specifying a molecular orientation state, and furthermore that the exact same palette of molecular orientations are accessible whether, following tilt θ of the molecular plane, the second rotation is 'leaning' as in (*9*) or rotation about the bowstring, the choice made here.) The net in-plane component of **P** can then be calculated, giving the **E** field direction in the model. Then γ, the rotation of the **z**–**h** molecular tilt plane from the plane of incidence (POI), can be related to the experimental azimuthal angle φ, the angle between the POI and **E** (for a $P = 0$ state, in which the film does not respond to **E**, γ is not defined absolutely). The 4 × 4 matrix calculations showed that for the very thin films studied here, with $Nd << \lambda$, the depolarised reflectivity of a point on a film could be obtained with adequate precision by calculating an effective **ε** for each layer and averaging through the film, which is to say that the relative ordering of the layers through the film does not affect

significantly the net $R_N(\chi,\beta,\gamma)$. This insensitivity to ordering of the layers is a feature of the depolarised reflectivity. The depolarised transmission measured via ellipsometry does depend on the ordering (*21*).

6. Conclusion

Study of the optical symmetry of the high-temperature liquid crystal phase of **NORABOW** produces the first direct evidence for a material having fluid layers with internally stabilised triclinic symmetry, exhibiting the SmCPG structure: spontaneous in–plane polar ordering as well as substantial coherent molecular tilt in two Euler angles, tilt of the long molecular axis $\theta \approx 38°$, and rotation about the long molecular axis $\chi \approx 16°$, giving an optical dielectric tensor with none of the principal axes oriented in or normal to the layer plane. This triclinic layer structure is found to be robust, depending little on the relative state of neighbouring layers or position relative to the air interface. Comparison shows that the layers of **NOBOW** strongly resist deformation from the SmCP structure, whereas **NORABOW** layers strongly resist deformation from the SmCG structure. The preferred bulk **NORABOW** phase is Sm CPG_A, i.e. with *G* rotations in opposite directions in adjacent layers.

Acknowledgements

This work was supported by NSF Materials Research Science and Engineering Center Grant DMR 0820579, NASA grant NAG3-2457, and NSF Grant DMR 0606528.

References

(1) deGennes, P.G. *The Physics of Liquid Crystals*; Oxford University Press: London, 1975; p 281.
(2) International Tables for Crystallography, Vol. A, Table 4.3.1; Kluwer Academic Publishers: Dordrecht/Boston/London, 1983.
(3) Meyer, R.B., Liebert, L., Strzelecki, L., Keller, P. *J. de Phys.* **1975**, *36*, L69–L71.
(4) Bahr, Ch., Fliegner, D. *Phys. Rev. Lett.* **1993**, *70*, 1842–1845.
(5) Young, C.Y., Pindak, R., Clark, N.A., Meyer, R.B. *Phys. Rev. Lett.* **1978**, *40*, 773–776.
(6) Walba, D.M., Körblova, E., Shao, R., Clark, N.A. *J. Mat. Chem.* **2001**, *11*, 2743–2747.
(7) Niori, T., Sekine, T., Watanabe, J., Furukawa, T., Takezoe, H. *J. Mat. Chem.* **1996**, *6*, 1231–1233.
(8) Link, D.R., Natale, G., Shao, R.F., Maclennan, J.E., Clark, N.A., Körblova, E., Walba, D.M. *Science* **1997**, *278*, 1924–1927.
(9) Pelzl, G., Diele, S., Weissflog, W. *Adv. Mater.* **11**, 707–724 (1999).
(10) Olson, D.A. *et al. Phys. Rev. E*, **2001**, *63*, 041702; Olson, D.A., Cady, A., Weissflog, W., Nguyen, H.T., Huang, C.C. *Phys. Rev. E,* **2002,** *64*, 015713.
(11) Jákli, A., Krüerke, D., Sawade, H., Heppke, G. *Phys. Rev. Lett.* **2001**, *86*, 5715–5718.
(12) Jákli, A., Nair, G., Sawade, H., Heppke, G. *Liq. Cryst.* **2003**, *30*, 265–271.
(13) Eremin, A., Diele, S., Pelzl, G., Nádasi, H., Weissflog, W. *Phys. Rev. E* **2003**, *67*, 021702.
(14) Jákli, A., Krüerke, D., Nair, G. *Phys. Rev. E* **2003**, *67*, 051702.
(15) Rauch, S., Bault,P., Sawade, H., Heppke, G., Nair, G., Jákli, A. *Phys. Rev.* E **2002**, *66*, 021706.
(16) Bedel, J.P., Rouillon, J.C., Marcerou, J.P, Nguyen, H.T., Achard, M.F. *Phys. Rev.* E **2004**, *69*, 061702.
(17) Gorecka, E., Pociecha, D., Vaupotic, N., Cepic, M., Gomola, K., J. Mieczkowski, J. *J. Mater. Chem.*, **2008**, *18*, 3044–3049.
(18) Hough. L., *et al. Science* **2009**, *325*, 452–456.
(19) Coleman, D.A. *et al. Science* **2003**, *301*, 1204–1211.
(20) Pindak, R., Young, C.Y., Meyer, R.B., Clark, N.A. *Phys. Rev. Lett.* **1980**, *45*, 1193–1196.
(21) Brand, H.R., Cladis, P.E., and Pleiner, H. *Eur. Phys. J. B* **1998**, *6*, 347–353.
(22) Walba, D.M. *et al. Science* **2000**, *288*, 2181–2184.
(23) Nakata, M. *et al. Liq. Cryst.* **2001**, *28*, 1301–1308.
(24) Chattham, N., *et al. Phys. Rev. Lett.* (submitted).
(25) Link, D.R., Maclennan, J.E., Clark, N.A. *Phys. Rev. Lett.* **1996**, *77*, 2237–2240.
(26) Jákli, A., Rauch, S., Lotzsch, D., Heppke, G. *Phys. Rev. E* **1998**, *57*, 6737.
(27) Pang, J.Z., Muzny, C.D., Clark, N.A. *Phys. Rev. Lett.* **1992**, *69*, 2783–2786.
(28) Berreman, D.W. *J. Opt. Soc. Am.* **1972**, *62*, 502–510.
(29) Olson, D.A., Han, X.F., Johnson, P.M., Cady, A., Huang, C.C. *Liquid Crystals* **2002**, *29*, 1521–1528.
(30) Hough. L., *et al. Science* **2009**, *325*, 456–460.